AD-A109 832 NAVAL RESEARCH LAB WASHINGTON DC F/G 8/3
SURFACE WAVE STATISTICS AND SPECTRA DURING HIGH SEA STATE CONDI--ETC(U)
DEC 81 C R MCCLAIN, D T CHEN, W D HART
UNCLASSIFIED NRL-MR-4722 NL

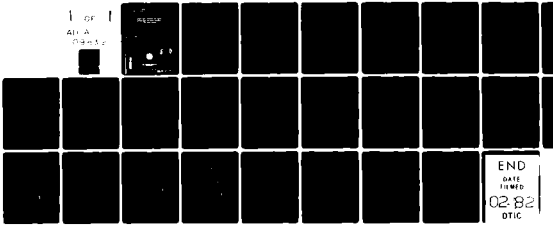

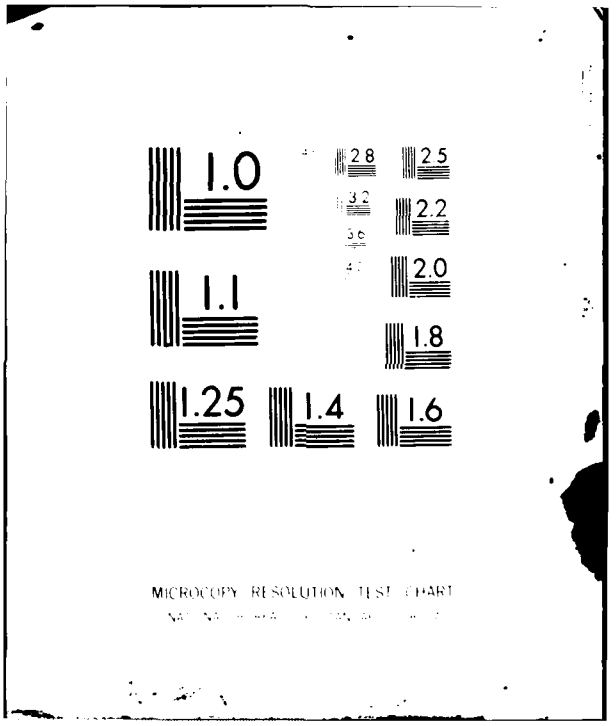
1.0
2.8
2.5
3.2
2.2
3.6
2.0
1.1
1.8
1.25
1.4
1.6
MICROCOPY RESOLUTION TEST CHART

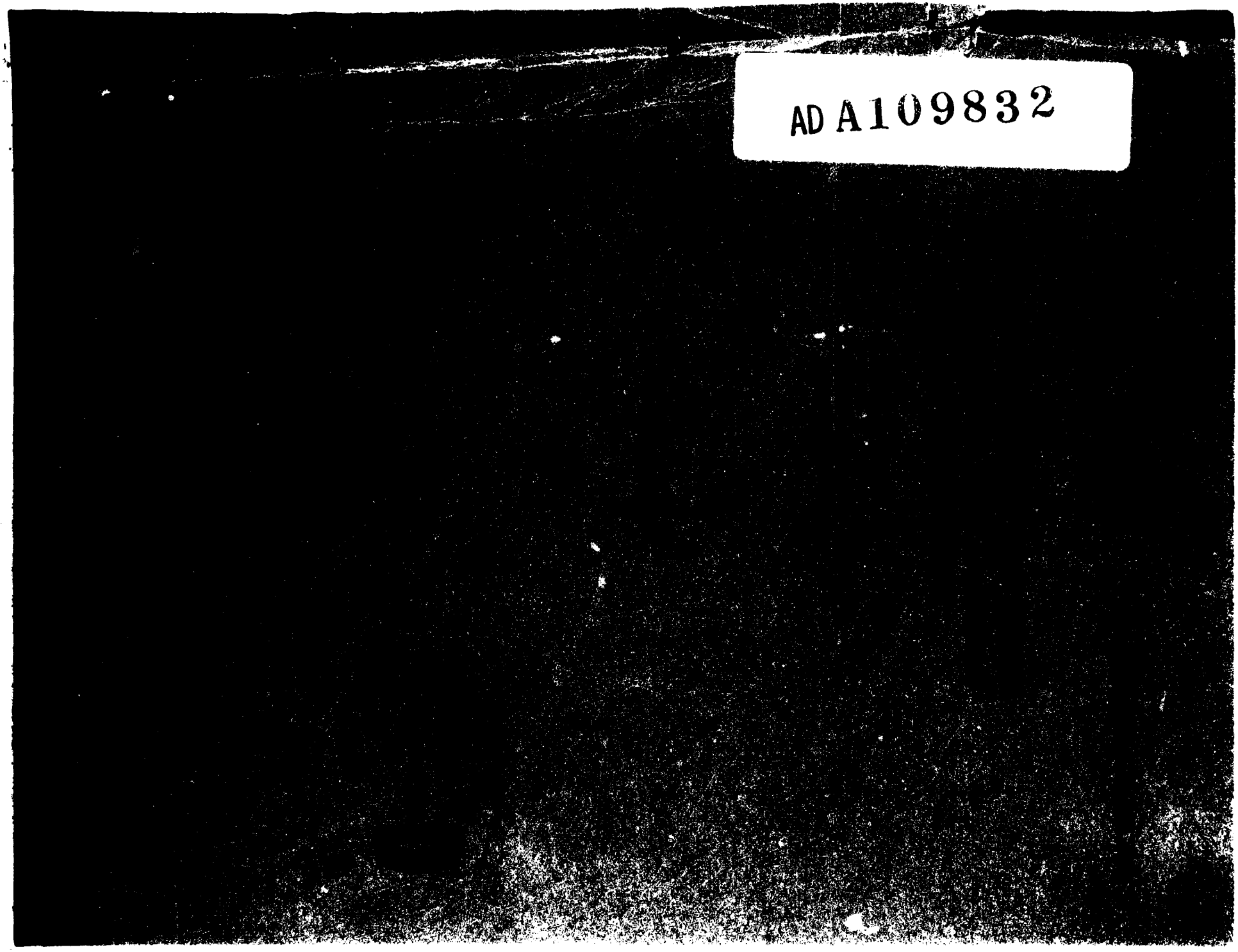

SECURITY CLASSIFICATION OF THIS PAGE (When Data Entered)

REPORT DOCUMENTATION PAGE		READ INSTRUCTIONS BEFORE COMPLETING FORM
1. REPORT NUMBER NRL Memorandum Report 4722	2. GOVT ACCESSION NO. AD-A101832	3. RECIPIENT'S CATALOG NUMBER
4. TITLE (and Subtitle) SURFACE WAVE STATISTICS AND SPECTRA DURING HIGH SEA STATE CONDITIONS IN THE NORTH ATLANTIC		5. TYPE OF REPORT & PERIOD COVERED Interim report on a continuing NRL problem. 6. PERFORMING ORG. REPORT NUMBER
7. AUTHOR(s) C.R. McClain*, D.T. Chen, and W.D. Hart†		8. CONTRACT OR GRANT NUMBER(s)
9. PERFORMING ORGANIZATION NAME AND ADDRESS Naval Research Laboratory Washington, DC 20375		10. PROGRAM ELEMENT, PROJECT, TASK AREA & WORK UNIT NUMBERS 61153N; RR032-08-41; 79-0930-0 & 62759N; WF59-553-000; 79-0928-0
11. CONTROLLING OFFICE NAME AND ADDRESS		12. REPORT DATE December 30, 1981 13. NUMBER OF PAGES 33
14. MONITORING AGENCY NAME & ADDRESS(if different from Controlling Office)		15. SECURITY CLASS. (of this report) UNCLASSIFIED 15a. DECLASSIFICATION/DOWNGRADING SCHEDULE

16. DISTRIBUTION STATEMENT (of this Report)

Approved for public release; distribution unlimited.

17. DISTRIBUTION STATEMENT (of the abstract entered in Block 20, if different from Report)

18. SUPPLEMENTARY NOTES

*Present address: NASA Goddard Space Flight Center, Greenbelt, MD 20771.
†Present address: Science Systems and Applications, Inc., Lanham, MD 20801.

19. KEY WORDS (Continue on reverse side if necessary and identify by block number)

Surface waves
Wave spectra
Wallops spectral model
Significant slope
Skewness
Airborne laser profilometer

20. ABSTRACT (Continue on reverse side if necessary and identify by block number)

Surface wave data collected using an airborne laser profilometer during high sea state conditions are analyzed to produce statistical cumulants up to the fifth order and power spectra. Theoretically, the third cumulant, skewness, is directly proportional to the wind-wave significant slope. This relationship is supported by wind-wave tank data, but little field data of this kind is available in the literature. Also, it has been suggested that if skewness can be derived from radar altimeter data, the significant slope would be

(Continues)

DD FORM 1 JAN 73 1473 EDITION OF 1 NOV 65 IS OBSOLETE
S/N 0102-014-6601

SECURITY CLASSIFICATION OF THIS PAGE (When Data Entered)

20. ABSTRACT (Continued)

computed and together with another altimeter product, the rms wave height, the wave spectra can be estimated using the Wallops Spectral Model (WSM). The results of this study indicate that the skewness relationship is valid for wind-wave dominated seas but as the swell contribution to rms wave height increases, the combined wave field skewness monotonically decreases below the predicted value. The WSM yields excellent reproductions of the wind-wave spectra even in multiple-peaked seas providing that the model inputs are properly determined for the wind-wave subfield. Finally the altimeter-WSM scheme should work reasonably well when the seas are wind-wave dominated provided that the altimeter can accurately measure skewness. More research on intermediate and swell dominated conditions is recommended.

CONTENTS

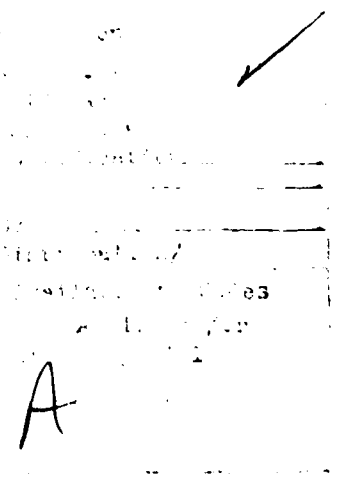

SURFACE WAVE STATISTICS AND SPECTRA DURING HIGH SEA STATE CONDITIONS IN THE NORTH ATLANTIC

1. INTRODUCTION

The simplest approach to remotely measuring surface waves is by profiling them from an aircraft along a line. This was discussed by Longuet-Higgins [1956] but few results using the technique were published until Barnett and Wilkerson [1967]. Since then, several studies have been conducted mostly on wind-generated wave fields. Most notable works are by Schule et al. [1971] and several by Ross including a recent study on Lake Michigan [Liu and Ross, 1980].

The use of airborne platforms offers several advantages and in the case of the profilometer, some disadvantages. Large areas can be surveyed in a short amount of time allowing flexibility in sampling schemes especially in complex or inhomogeneous wave fields. Perhaps the most important advantages of profilometry are the ease of deployment, the reliability of hardware, and the simplicity of the analysis as compared to most other devices that can be used in deep water. Examples of situations where the mobility of airborne profilometry is of definite advantage is for sea truthing other remote sensors, especially spaceborne, and in wind wave, wave-current and perhaps wave-bottom interaction studies. The disadvantages are that the seas rarely consist of purely swell or purely wind driven seas and, therefore, any one flight track will result in aliasing of at least one major component. This can be overcome somewhat by flying several tracks in a pattern. Also, in cases where sharp changes in sea state occur, the spectrum may not show the true surface change since a finite distance is required to generate an average spectrum with a reasonable number of degrees of freedom and therefore, smoothing results.

The data set used in this report was collected for the purpose of validating the GEOS-3 radar altimeter significant wave height ($H_{1/3}$) estimates. Initial results from that experiment in 1976 have been published by McClain et al. [1979]. The data set consists of six missions flown during high sea states and is of sufficient quality to allow the testing of more recent theoretical and empirical results which imply that additional information may be extracted from altimeter data.

According to the theoretical development by Longuet-Higgins [1963], the third cumulant and therefore the skewness of the distribution of surface elevation can be evaluated in terms of the frequency spectrum. This formalism has been applied by Huang and Long [1980] who incorporated the analytical form of the Phillips spectrum. The result was a linear relationship between skewness and significant slope (rms wave height/dominant wavelength). The relationship was corroborated by their wind-wave tank data. Longuet-Higgins on the other hand applied his analysis to field data by Kinsman [1960] and did not incorporate any theoretical models of the wave spectrum into his analysis. It is important to note that measurements of skewness in the literature are rare.

Manuscript submitted November 20, 1981.

Over the past thirty years, a great amount of effort has been directed towards finding an analytical expression for the wave spectrum. The most recently proposed model is the Wallops Spectral Model (WSM) by Huang et al. [1981]. This model requires two inputs, the rms wave height and the dominant wavelength. Like previous models, it assumes that the wave field has only one dominant component and is not a superposition of swell and wind waves with comparable energies.

Besides being mathematically simple in form and requiring only two inputs, the model has an interesting connection to satellite radar altimetry which couples with the skewness relationship. Walsh [1979] has shown that it may be possible to measure skewness with an altimeter. His results were derived from GEOS-III data and although his results will be critically discussed later, the possibility has been demonstrated. For the purposes of this paper, it is assumed that accurate measurement of skewness from an altimeter is possible since an altimeter such as the one on SEASAT provides much more accurate and detailed information on the return waveform. Also, the rms wave height has been proven to be a reliable measurement from an altimeter [Parsons, 1979]. Thus, by applying the skewness relationship, the dominant wavelength can be estimated and together with the rms waveheight, the ocean wave spectrum can be calculated using the WSM.

It is the intention of this paper to present results, derived from airborne profilometer measurements of surface waves, and to compare them with those predicted by Huang and Long [1980] and Huang et al. [1981]. In particular, we want to test the relationship between skewness and significant slope for a variety of combinations of sea and swell. Secondly, we want to investigate the possibility of using skewness measurements for calculating parameters in the Wallops model. Finally, we want to check the spectral model when the parameters are calculated from field data with swell effects removed.

2. REVIEW OF THEORY

Huang and Long [1980] have shown that the available skewness data compares very well to the theoretical relationship,

$$K_3 = 8\pi\xi \tag{1}$$

where K_3 is the skewness of the surface wave elevation distribution relative to the mean sea level and ξ is the significant wave slope which is defined as

$$\xi = (\bar{\zeta^2})^{1/2}/\lambda_o \tag{2}$$

$\bar{\zeta^2}$ is defined as the mean square surface elevation relative to the mean sea level and λ_o is defined as the dominant wavelength at the peak of the ocean wave spectrum. From (1) the significant wave slope ξ can be evaluated if the value of skewness K_3 is known from the measurement.

Furthermore, from the mean square surface wave amplitude and (2), the dominant wavelength λ_o will be calculated. Knowledge of the value of ξ and λ_o are essential to construct the WSM. Considering, a single train of waves the slope m of the line connecting the principle and the first harmonic waves in the Stoke's expansion should be

$$m = \left| \frac{\log(2ak_o)^2}{\log\ (1/2)} \right| \tag{3}$$

Extending this result to a broader band wave spectrum which is a better representation of the random wave field, (3) will have the form of

$$m = \left| \frac{\log(\sqrt{2}\pi\xi)^2}{\log\ 2} \right| \tag{4}$$

since, for a random wave field,

$$\bar{\zeta}^2 = a^2/2 \tag{5}$$

and

$$k_o = \frac{2\pi}{\lambda_o} \tag{6}$$

Once the significant wave slope ξ is evaluated, from (4), m is known.

The Wallops wave spectral model has the form of

$$\phi(n) = \frac{\beta g^2}{n_o^5} (n_o/n)^m \exp\ [-\delta(n_o/n)^\eta] \tag{7}$$

where n_o is the wave frequency at the spectral peak, g is the gravitational acceleration, and β, δ and η are coefficient functions. Since $\partial\phi(n)/\partial n = 0$ at $n = n_o$, it is concluded that $m = \delta\eta$. If η is chosen to be 4 as did Pierson and Moskowitz [1964] and Hasselmann et al. [1976],

$$\delta = m/4 \tag{8}$$

Furthermore, with the definition of the spectral function as

$$\bar{\zeta}^2 = \int_0^\infty \phi(n)dn$$

and incorporation of the linear dispersion relationship of $n_o^2 = gk_o$,

$$\beta = \frac{(2\pi\xi)^2 m^{(m-1)/4}}{\Gamma\left(\frac{m-1}{4}\right) 4^{(m-5)/4}} \tag{9}$$

Where Γ is the Gamma function. Therefore, from (4) to (9), the Wallops wave spectral model is

$$\phi(n) = \frac{\beta g^2}{n^m n_o^{(5-m)}} \exp\left[-\frac{m}{4}(n_o/n^4\right] \qquad (10)$$

Following the theoretical work laid out by Longuet-Higgins [1963], the theoretical bounds of the skewness are

$$5.28\pi\xi(m-1)/(m-2) \leq K_3 \leq 12.12\pi\xi(m-1)/(m-2) \qquad (11)$$

Equations (1) to (11) form the basic equations for the comparisons between the theoretical predictions and the measurements made during the experiment.

3. EXPERIMENT

An airborne experiment was conducted off the coast of Newfoundland, Canada, in February 1976 (see Figure 1). The original intent of the experiment was to collect aircraft measurements of Significant Wave Height (SWH) to be used to test and validate the performance of the GEOS-3 satellite altimeter algorithms. The experiment was conducted by the Space Sensing Applications Branch at the Naval Research Laboratory (NRL).

One of the instruments aboard the NASA Wallops Flight Center (NASA/WRC) C-54 aircraft was a Geodolite continuous wave laser. The significant wave height was reported to be 4.0 - 8.0 meters by Parsons [1979] and McClain et al. [1979]. For the present study, more refined analysis of the laser data resulted in improved values of significant wave height. Figure 2 is taken from McClain et al. [1979] but with the new laser values. The sea states during the six flights were generally high and were composed of various combinations at sea and swell. The wave profiles thus constitute a unique data set and is most appropriate for testing the general applicability of the relationships discussed in section 2.

4. DATA ANALYSIS

In order to measure statistical moments of higher order than the second, an improved approach implemented for removing aircraft motion from the profilometer record over that previously used [McClain et al., 1980] is required. The earlier approach was to incorporate verticle aircraft acceleration into the correction scheme by (a) filtering both laser and accelerometer records using the same filter (b) Fourier transforming them separately, (c) doubly integrating the acceleration power spectrum by dividing each component by a factor of $(2\pi f)^4$ where f is the frequency; and (d) subtracting that spectrum from the profilometer spectrum. To generate a corrected time series from which higher moments can be easily calculated, the double integration was performed in the time domain. Parabolic trends result and various techniques have been devised to remove them. Several schemes including a least squares curve fitting to a parabola were tested,

but it was found that by first subtracting the mean acceleration from the data segment, then double integrating and finally applying a numerical filter, the most satisfactory result was produced. The procedures were tested using artifically generated laser and accelerometer time series. Accelerometer data is used in both frequency and rime domain processing to remove residual vertical aircraft motion that the filter passes.

The filter is designed with a cut-off which allows reasonable wavelengths of encounter to pass. The final wave record is obtained by subtracting the filtered profilometer series from the final aircraft motion record since the laser measures the inverted surface. Also, it appears that the laser phase shift correction routine needed for this particular instrument can induce spurious long wavelength components making comparison of long data records of laser and aircraft motion difficult. A pulsed laser system such as is presently used by NRL measures absolute range and does not encounter this problem. Filtering removes this error source.

The filter used was a nonrecursive Martin filter [Martin, 1959] and its design for this application is discussed in McClain and Walden [1979]. It has the necessary property of zero phase shift since the weighting function is symmetric. Figure 3 provides the response function for the filter applied in all but one instance.

Before Fourier analysis, each data segment to be transformed was smoothed using a 4-term Blackman-Harris window as described in Harris [1978]. This window is characterized by one main lobe with a 6 dB band width of 2.7 bins and no side lobes. All final spectra were derived by averaging five spectra each being the Fast Fourier Transform (FFT) of 2048 points. The digitization rate was 45 Hertz. This corresponds to a distance, D, given by

$$D = \frac{(2048)}{45} \quad |\vec{U}| \tag{12}$$

where $\vec{U}$ is the ground velocity of the C-54 aircraft in meters per second. The slowest ground speed occurred for data set 2/23b, i.e., data set b on Feb. 23, and was 50 m/s. Therefore, D = 2.28 km or about nine dominant wavelengths on that day and the sample spacing was about 1 meter. It was felt that a transform of this size was appropriate in order to provide sufficient spectral resolution for our application, i.e., the determination of dominant wavelength.

The algorithm for true frequency, f_t, is based on the Doppler shift expression,

$$2\pi f_t = 2\pi f_a + \vec{k}_t \cdot \vec{U} \tag{13}$$

where f_a is the apparent frequency, $\vec{k}_t$ is the wave number vector associated with f_t, and $\vec{U}$ is the ground velocity of the aircraft. For sea states the size investigated and upwind ground speeds being rather slow, the

inclusion of f_t in (13) is necessary. For instance, the calculated f_t for the dominant wave component on 2/23b corresponds to a phase speed of approximately 20 m/s or 40% of the ground speed and negates any assumption that the surface is relatively stationary.

The facts that ground speed varies from one flight line to the next, that the transforms were uniform in size, and that (13) is nonlinear in f do lead to variable resolution in the frequency domain. The spectra from 2/23a and 2/23b exemplify this since the ground speed of 2/23a was 120 m/s.

For the flights on 2/20, 2/24, 2/28, and 3/3, significant amounts of swell were present. The algorithm assumes only one angle of encounter and since all flights were up or down wind, only the wind wave components were accurately mapped. Therefore, the points labeled swell are not accurately located, but no method to correct them is possible with a flight pattern with one leg. This problem is particularly bothersome on 2/24. The effect of sampling a directionally dispersed wind wave field with a line has been analytically studied in Hammond and McClain [1980] and is shown not to be a serious problem. The moments were generated from ungrouped data, i.e., the probability density functions were not determined. These values were used in determining the cumulants, K_n. The equations for the K_n's are the same as those in Huang and Long [1980].

5. RESULTS

The ocean wave spectra (Figures 4 through 9) can be typically classified into three types of sea states. The first type, represented by Figure 4 through 6 show the sea state is not only wind-generated but also contains wave energy from the swell. The dominant wind wave peak has been identified as W, and the dominant swell peak by S. Generally speaking, the total wave energy contained in the various swell components is not large in comparison with the total wave energy of the wind wave components. The significant wave height for 2/23a was 7.89 meters, and wave spectrum at high wave frequencies approached those predicted by Phillips [1958] assuming the equilibrium coefficient β to be 0.81×10^{-2}. The predicted peak value using Phillips model and the observed value for 2/23a are 152 and 153 $m^2 s$ respectively. The second type of ocean wave spectra is represented by Figure 7 for the date of 2/23b. The significant wave height was 8.7 meters and the sea state was purely wind-generated. The third type, represented by Figures 8 and 9, show that the sea is essentially swell.

The wave statistics and the hindcasts for all of these dates are presented in Table 1. The dominant wavelengths, λ_o, were obtained separately for the dominant swell and wind waves. In case there was inadequate information available, the space is left blank. A long bar indicates that no value was determined. The values of $H_{1/3}$, K_3, the fourth order cumulant K_4, the fifth order cumulant K_5, and hindcasts on wind vectors have been evaluated or observed for the combined sea; therefore, their values are not particularly associated with either swell or wind waves.

The significant slopes ξ as defined by (2) were calculated separately for wind waves and swell by using the combined rms wave amplitude shown in Column 3, and the dominant wavelengths for wind waves and swell as shown in Column 4. The values of $\lambda_o/H_{1/3}$ shown in Column 9 are one quarter of the inverse values of ξ. Various hindcast values of the wave field and winds are in Columns 10 and 11, respectively, and were taken from Mennella et al. (unpublished manuscript, 1976). In column 12, the equilibrium range slopes are estimated from Figures 4 through 9.

Figure 10 shows the plot of K_3 with respect to ξ. The data provided in Huang and Long [1980] are shown as small solid circles (wave tank) and Δ (field data from Kinsman). The solid curve represents the empirical relationship, (1). On the dates 2/28 and 3/3 two data points are shown. The data on the left indicates swell peaks and the data on the right indicates wind wave peaks. They are connected by a horizontal line whose length is an indication of the range of variation of ξ. As one can observe from Figure 10 the data points of the present study are coincident with those of Kinsman but have less scatter. The wavelength used for 2/24 is the hindcast value, since the flight track was parallel to the wind and apparently at a large angle to the swell. A special filter had to be applied in order to pass the aliases swell component.

At this point a comment regarding the results of Walsh [1979] is appropriate. The GEOS-3 data represented in that paper corresponds to our underflight data sets 2/20 and 2/23a. The skewness values determined by Walsh from the GEOS-3 altimeter were 0.21 and 0.54, respectively, as compared to our values of 0.11 and 0.20 derived from the profilometer. In order to evaluate ξ, the hindcast wavelengths used by Walsh were 150 m for 2/20 and 96 m for 2/23. Although we cannot determine the swell wavelength on 2/20 precisely, the wind wave peak was 96 m and on 2/23a the peak was 242 m. The 2/20 data was swell dominated. Therefore, it appears that the apparent agreement between Walsh's results and (1) occurred because the consistently over estimated K_3 was balanced by under estimation of λ_o. We find that the hindcast estimates of SWH (Figure 2) and of wavelength of period (Table 1) tend to be low at least for these data sets.

Figure 11 shows the plot of the fourth order cumulent K_4 with respect to ξ. Again the data points of the present study stay within the same range of ξ values as those of the other in situ field study but with less scatter. Figure 12 shows the plot of the fifth order cumulent with respect to the significant slope. The solid curve is the empirical relationship,

$$K_5 = -110\ \xi \qquad (14)$$

by Huang and Long [1980]. It should be noted, however, there is no in situ field data available. The values are well-behaved and comparatively uniform in value.

In order to illustrate more effectively the skewness dependence, a linear plot with respect to $\lambda_o/H_{1/3}$ (Column 9 in Table 1) is shown in Figure 13. The dashed curves are the theoretical upper and lower bounds,

as shown by (11). The Δ points are defined later. Because various proportions of the total wave energy are contributed by swell, the data points for the date of 3/3 are outside the bounds. The data points of 2/24 are not included here. Otherwise, the data points for the remaining dates are reasonably predicted by (1), and the theoretical bounds. Since the significant wave height used includes both the swell and wind wave contributions, it is indeed arguable whether or not this is a fair comparison. Longuet-Higgins' [1963] original derivation should be applicable for the combined sea state, but the theoretical curves were derived by using a continuous wave spectrum extending from the dominant wave through the high frequency wave domain.

If skewness and rms waveheight are the measured quantities, all of the terms in the Wallops spectral model can be calculated and compared with the values in Table 1. This procedure simulates an altimeter-derived product. Table 2 shows the parameters derived from (1), (2), (4), and (9) using the values of skewness and $H_{1/3}$ of Table 1. The spectra shown in Figure 15 are two modeled spectra and a profilometer spectrum. The model spectrum derived from direct evaluation of dominant wavelength and rms wave height shows excellent agreement. The second modeled spectrum is derived using the measured K_3 and (1). The fit is not bad although the dominant wavelength is now only 198 m.

Of particular interest to the current study is the consideration of cases where the effects due to swell on $H_{1/3}$, ξ, m, β, λ_o, n_o, and f_o are removed. From the ocean spectra it is easy to remove the swell contributions to the root mean squared surface wave amplitudes. The arrows in Figures 4 to 9 indicate the separation of sea and swell. The separation point was determined by the slope of the equilibrium range and by using the hindcast predictions of seas and swell. The result of this separation is given as E_s/E, the ratio of swell energy to total energy and is listed in Table 1. The relationship of significant wind wave height to this quantity is

$$H^w_{1/3} = (1 - \frac{E_s}{E})^{1/2} H_{1/3} \qquad (15)$$

Using the observed wind wave peaks, n^w_o is known and Table 3 can be generated. The superscript W indicates Wind Waves.

The skewness contribution due to swell is difficult to evaluate and cannot be easily separated in these data since the swell is mismapped. Such a separation would assume that the swell does not interact with the wind-wave field. Perhaps a calculation of the bispectrum (Hasselmann, et al, 1973) would be useful. In order to evaluate the effect of swell in a quantitative manner, $H^w_{1/3}/\lambda^w_o$ is calculated from Table 3 and plotted as Δ on Figure 13. Using (1) or the solid curve in Figure 13, the predicted values of skewness K'_3 is determined. Figure 15 is a plot of the difference between the measured and the predicted skewness, $K_3 - K'_3$, as a function of E_s/E. A trend seems to exist. Figure 16 presents the standard deviation of the K_3 estimates for each data set as a function of E_s/E. As expected, the variabilities in K_3 are relatively high

compared to the mean values but the standard deviations are similar to those of the tank data in Figure 10. No apparent trend is seen in Figure 16.

Finally, using the parameters in Table 3, a comparison of the wind-wave portion of 3/3 and the model is shown in Figure 17. The fit is quite good and illustrates the point that subfields can be modeled independently and the wave-wave interaction between swell and the wind-wave field are weak.

6. CONCLUSIONS

Regarding skewness, the data, though limited, tends to support the skewness relation, (1), even with moderate amounts of swell present. However, as the swell contribution to total energy increases, larger deviations result. This is expected since swell should be more Gaussian. Computation of K_4 and K_5 help demonstrate the reliability of these measurements by comparing favorably with other data and exhibiting values appropriate to nearly Gaussian processes. More data from swell-dominated seas needs to be analyzed and large quantities probably exist but are left unstudied since most interest has been in wind wave generation.

Comparisons of the WSM and measured spectra show excellent agreement and indicate that sub-fields can be modeled independently. Also, the feasibility of using the skewness and rms height measurements from an altimeter to infer wave spectra using the WSM is promising, especially in wind-wave dominated seas. These seas are of greater practical interest to mariners and for wave forecasting. It remains to be proven, however, that the altimeter can accurately measure skewness.

ACKNOWLEDGEMENTS

This work is supported by NRL RR032-08-41 Program Element 61153N32 and NAVAIR WF 59-553-000 Program Element 62759N to NRL, and is also support by NASA Goddard Space Flight Center RTOP 146-40-15-25.

The authors would like to thank Dr. Norden Huang of NASA/WFC and Dr. Frederick Jackson of NASA/GSFC for many discussions and their recommendations.

REFERENCES

Barnett, T. P. and J. C. Wilkerson, On the Generation of Ocean Waves as Inferred from Airborne Radar Measurements of Fetch-Limited Spectra, Journal of Marine Research, 25, 292-328, 1967.

Hammond, D. L. and C. R. McClain, Spectral Distortion Inherent in Airborne Profilometer Measurements of Ocean Wavelengths, Ocean Engineering, 7, 99-108, 1980.

Harris, F. J., On the Use of Windows for Harmonic Analysis with the Discrete Fourier Transform, Proceedings, IEEE, 66(1), 51-83, 1978.

Hasselmann, K., W. Munk and G. McDonald, Bispectra of Ocean Waves, Time Series Analysis, Edited by M. Rosenblatt, John Wiley & Sons, New York, 1963.

Hasselmann, K., D. B. Ross, P. Muller and W. Sell, A Parametric Wave Prediction Model, Journal of Physical Oceanography, 6, 200-228, 1976.

Huang, N. E. and S. R. Long, An Experimental Study of the Surface Elevation Probability Distribution and Statistics of Wind-Generated Waves, Journal of Fluid Mechanics, 101, 179-200, 1980.

Huang, N. W., S. R. Long, C. C. Tung, Y. Yuen, and L. F. Bliven, A Unified Two-Parameter Wave Spectral Model for a General Sea State, Journal of Fluid Mechanics, in press, 1981.

Kinsman, B., Surface Waves at Short Fetches and Low Wind Speed - A Field Study, Chesapeake Bay Inst., Johns Hopkins University Technical Report 19, 1960.

Liu, P. C. and D. B. Ross, Airborne Measurements of Wave Growth for Stable and Unstable Atmospheres in Lake Michigan, Journal of Physical Oceanography, 10(11), 1842-1853, 1980.

Longuet-Higgins, M. S., The Statistical Analysis of a Random, Moving Surface, Philosophical Transactions, Royal Society of London A, 249, 321-387, 1956.

Longuet-Higgins, M. S., The Effect of Non-Linearities on Statistical Distributions in the Theory of Sea Waves, Journal of Fluid Mechanics 17, 459-480, 1963.

Martin, M. A., Frequency Domain Applications to Data Processing, IRE Transactions on Space Electronics and Telemetry, 13-41, 1959.

McClain, C. R., D. T. Chen and D. L. Hammond, Comment on "GEOS-3 Wave Height Measurements: An Assessment During High Sea State Conditions in The North Atlantic", by C. L. Parsons, Journal of Geophysical Research, 84(B8), 4027-4028, 1979.

McClain, C. R. and H. Walden, On the Performance of the Martin Digital Filter for High and Low Pass Applications, NASA TM-80593, 1979.

McClain, C. R., D. T. Chen and D. L. Hammond, Gulf Stream Ground Truth Project: Results of the NRL Airborne Sensors, Ocean Engineering, 7, 55-97, 1980.

Parsons, C. L., GEOS-3 Wave Height Measurements: An Assessment During High Sea State Conditions in the North Atlantic, Journal of Geophysical Research, 84(B8), 4011-4020, 1979.

Phillips, O. M., The Equilibrium Range in the Spectrum of Wind Generated Waves, Journal of Fluid Mechanics, 4, 46-434, 1958.

Pierson, W. J., Jr. and L. Moskowitz, A Proposed Spectral Form for Fully Developed Wind Sea Based on the Similarity Theory of S.A. Kitaigorodskii, Journal of Geophysical Research, 69, 5181-5190, 1964.

Schule, J. J., Jr., L. S. Simpson and P. S. DeLeonibus, A Study of Fetch-Limited Wave Spectra with an Airborne Laser, Journal of Geophysical Research, 76, 4160-4171, 1971.

Walsh, E. J., Extraction of Ocean Wave Height and Dominant Wave Length from GEOS-3 Altimeter Data, Journal of Geophysical Research, 84(B8), 4003-4010, 1979.

Table 1 - Wave Statistics and Hindcasts from Profilometer. T, Wave Period in Seconds; E_s, Wave Energy Due to Swell; E, Total Wave Energy

DATE	SEA STATE	$H_{1/3}$	λ_o	K_3	K_4	K_5	Eq. (2) ξ	$\lambda_o/H_{1/3}$	HINDCAST $H_{1/3}/T$	WIND, SPEED/HEADING	m	E_s/E
2/20	SWELL WIND WAVE	4.74	273 90	0.1098	-0.0957	0.1475	0.00434 0.0132	57.59 19.00	4.5/10 0.5/3	9/281°	4.91	0.74
2/23a	SWELL WIND WAVE	7.89	242	0.1981	0.0196	-0.0883	0.00813	30.67	2/14 7/7	22/229°	4.91	0.24
2/23b	SWELL WIND WAVE	8.68	--- 262	0.2753	-0.0275	-0.1343	--- 0.00828	--- 30.18		22/229°	5.07	0.00
2/24	SWELL WIND WAVE	5.10	--- 112	-.1000	-0.1700	0.3800	0.042 0.0114	60.00 22.00	5/14 1.5/4	6/296°	4.13	0.84
2/28	SWELL WIND WAVE	4.47	262 110	0.1336	-0.1601	-0.1309	0.00427 0.01016	58.61 24.61	0.5/15 4/6	19/148°	5.11	0.29
3/3	SWELL WIND WAVE	5.51	203 116	0.0800	-0.0900	0.3400	0.00676 0.0045	36.84 55.00	1/12 4.5/8	12.5/274° 15 Previously	5.10	0.30

Table 2 - Parameters for Probability Distributions and Spectra

DATE	SEA STATE	Eq. (1) ξ	Eq. (4) m	Eq. (9) $\beta \times 10^2$	Eq. (2) λ_o	n_o	f_o
2/20	SWELL AND WIND WAVE	0.00437	11.37	3.18	271	0.4767	0.0759
2/23a	SWELL AND WIND WAVE	0.00788	9.67	6.14	250	0.4963	0.0790
2/23b	SWELL AND WIND WAVE	0.01095	8.72	8.76	198	0.5577	0.0888
2/24				NO ENTRIES			
2/28	SWELL AND WIND WAVE	0.00532	10.81	3.98	210	0.5415	0.0862
3/3	SWELL AND WIND WAVE	0.00318	12.3	2.23	433	0.4490	0.0714

Table 3 - Revised Parameters for Wind Wave Spectra by Removing the Effects of Swell on Sea State

DATE	SEA STATE	$H^{w}_{1/3}$	λ_o	ξ	$\lambda_o/H_{1/3}$	Eq. (4) m	Eq. (9) β	n_o	f_o
2/20	WIND WAVE	2.42	90	0.00672	37.2	10.10	5.10×10^{-2}	0.830	0.132
2/23a	WIND WAVE	6.88	242	0.00711	35.2	10.06	4.72×10^{-2}	0.503	0.080
2/23b	WIND WAVE	8.68	262	0.00828	30.18	9.53	6.49×10^{-2}	0.484	0.077
2/24	WIND WAVE	2.01	112	0.00449	55.7	11.30	3.30×10^{-2}	0.741	0.118
2/28	WIND WAVE	3.79	110	0.00861	29.0	9.42	6.77×10^{-2}	0.748	0.119
3/3	WIND WAVE	4.61	203	0.00568	44.0	10.62	4.27×10^{-2}	0.550	0.088

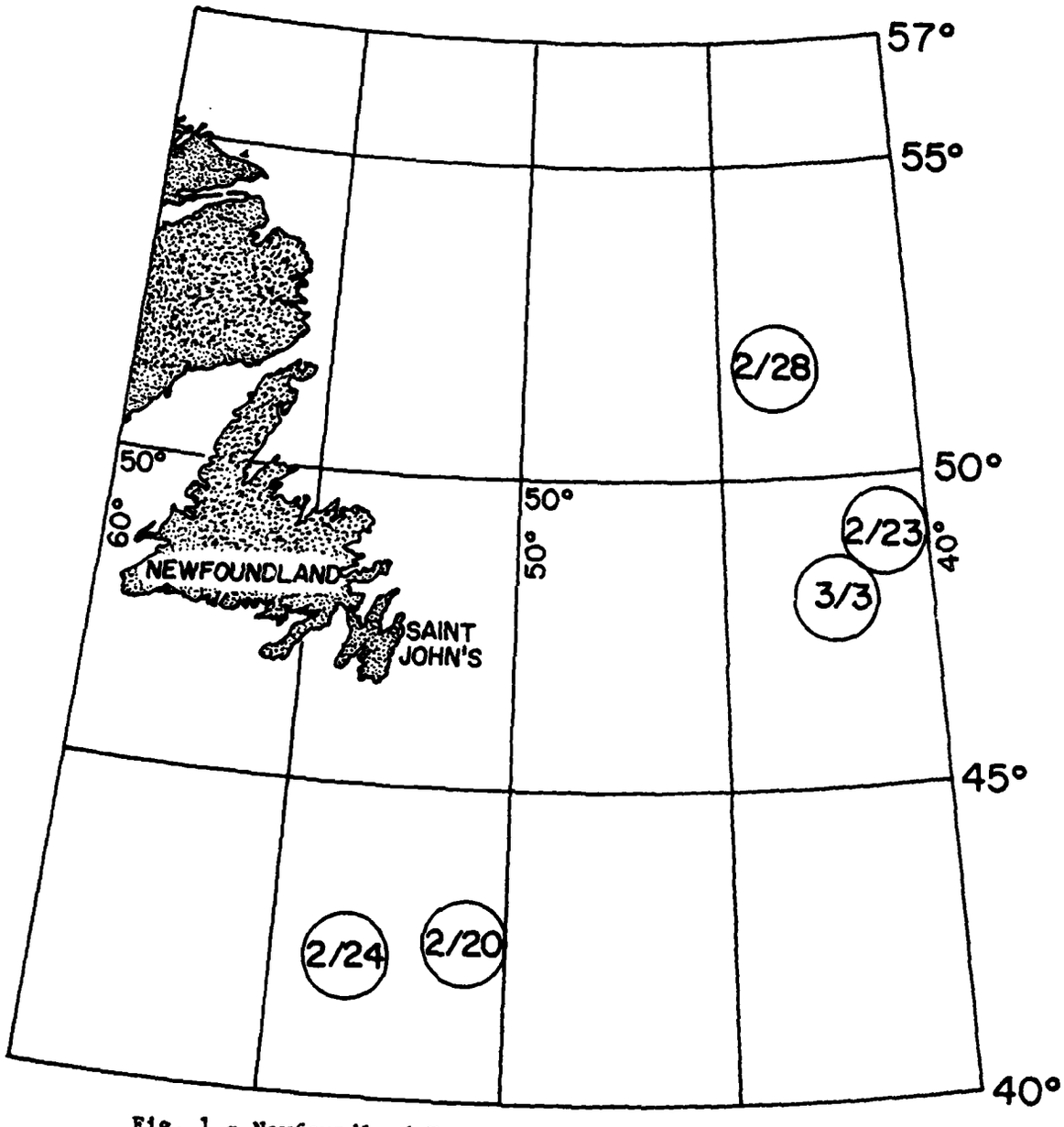

Fig. 1 - Newfoundland Experiment Underflight Locations

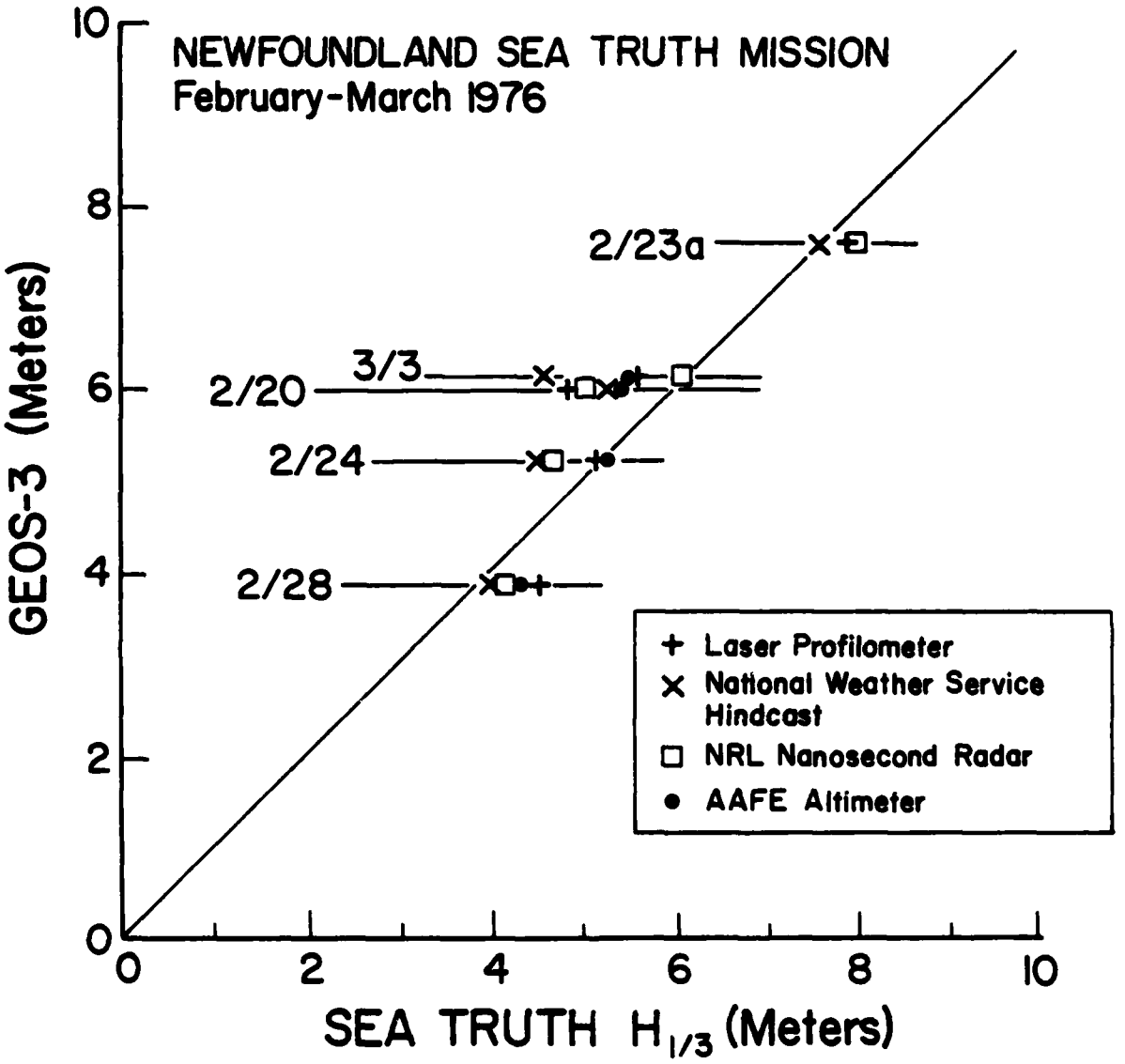

Fig. 2 - Comparison of GEOS-3 and Sea Truth Significant Wave Heights

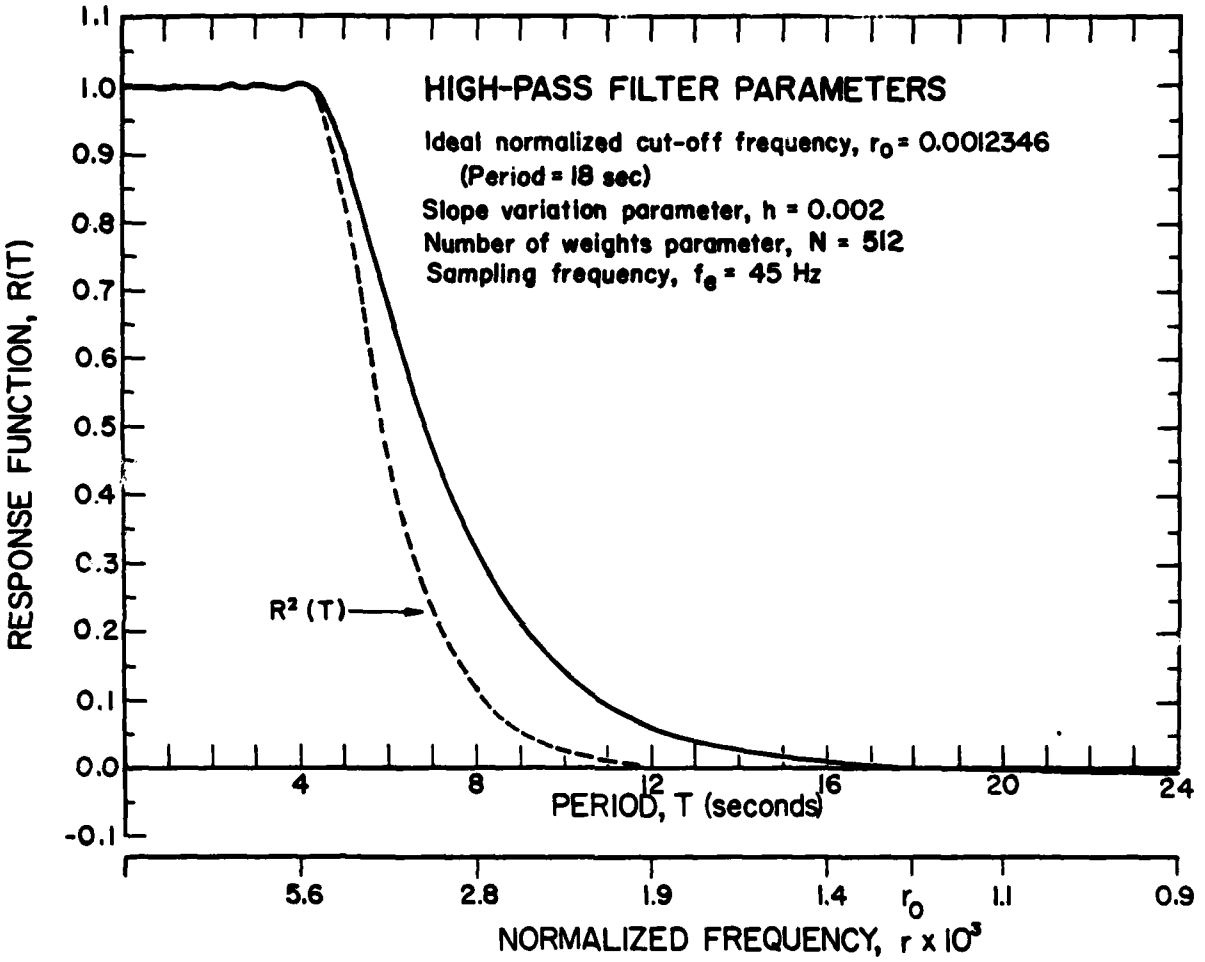

Fig. 3 - Response Function for the Filter

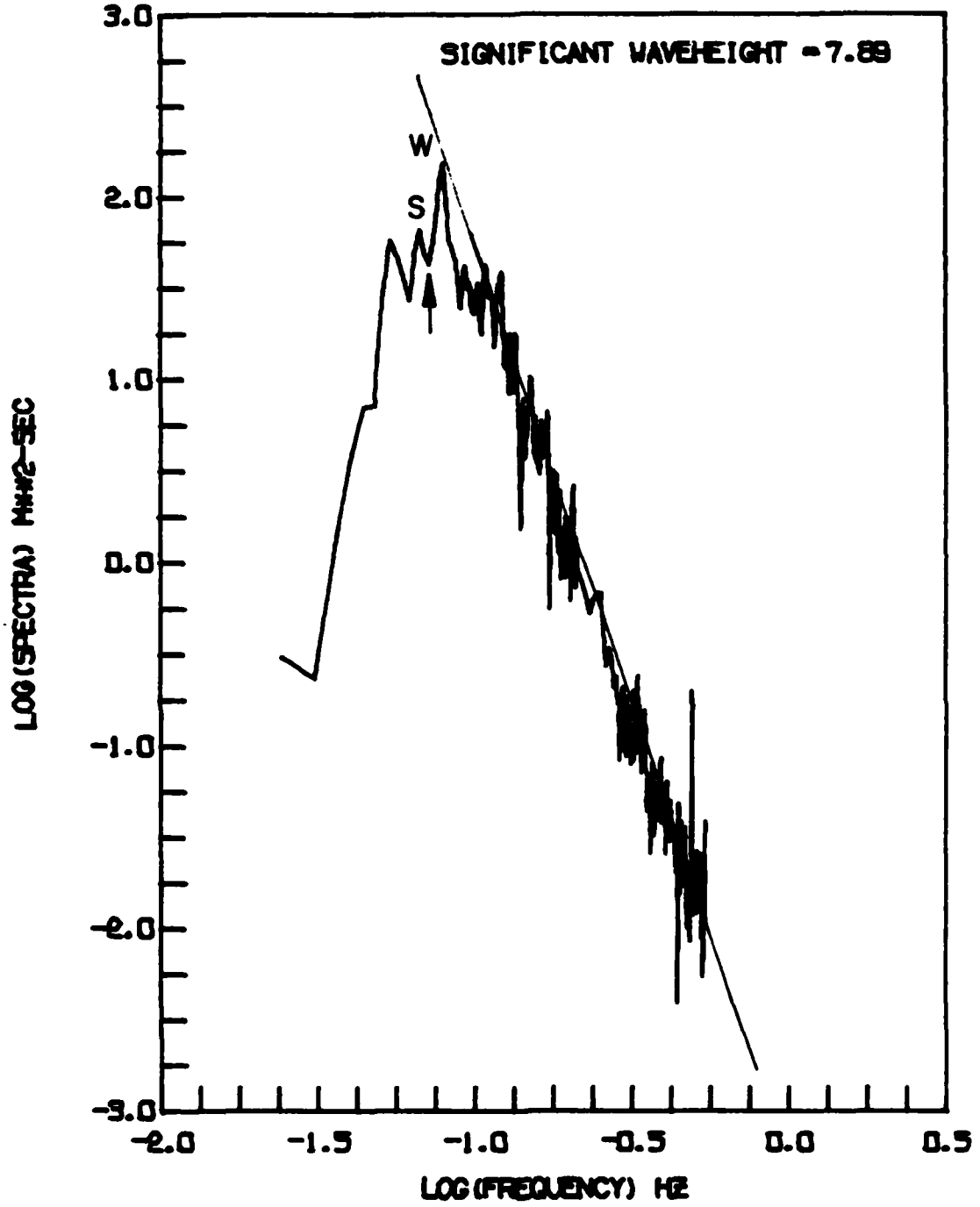

Fig. 4 - Ocean Wave Spectrum, Feb. 23a, 1976. W, Wind Wave Peak; S Swell Peak; ↑, Separation of Swell and Wind Wave

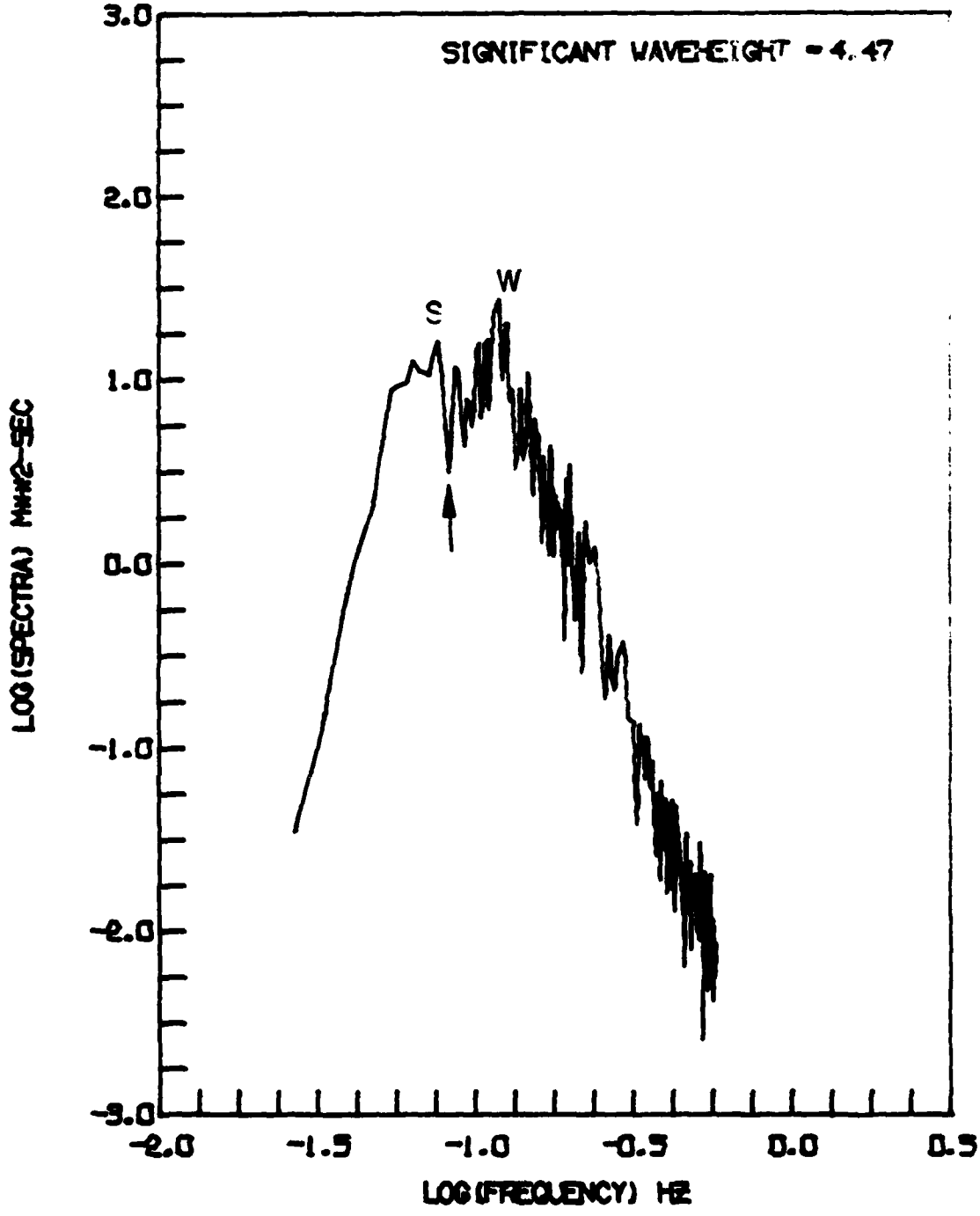

Fig. 5 - Ocean Wave Spectrum, Feb. 28, 1976. For legend, see Fig. 4

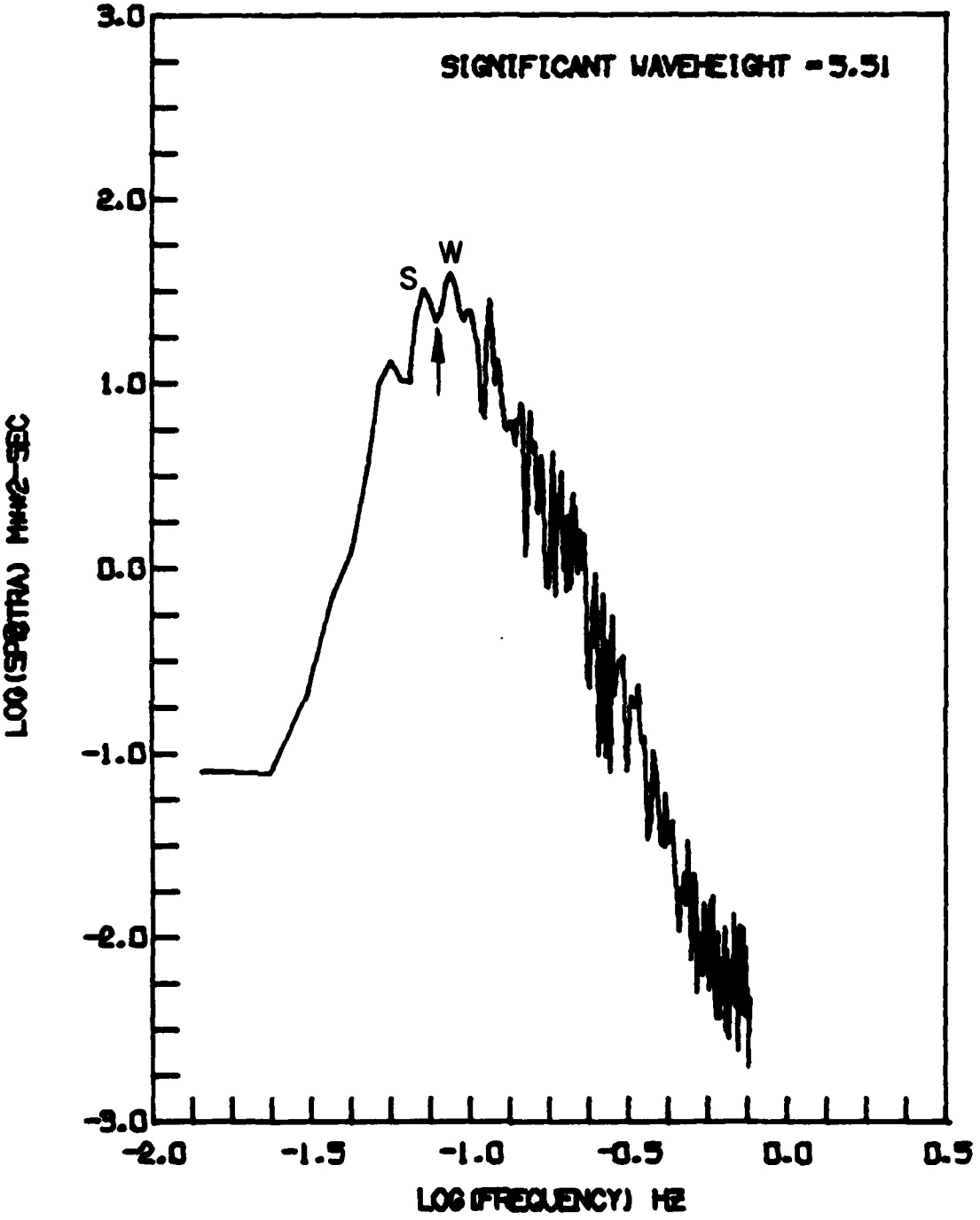

Fig. 6 - Ocean Wave Spectrum, March 3, 1976. For legend, see Fig. 4

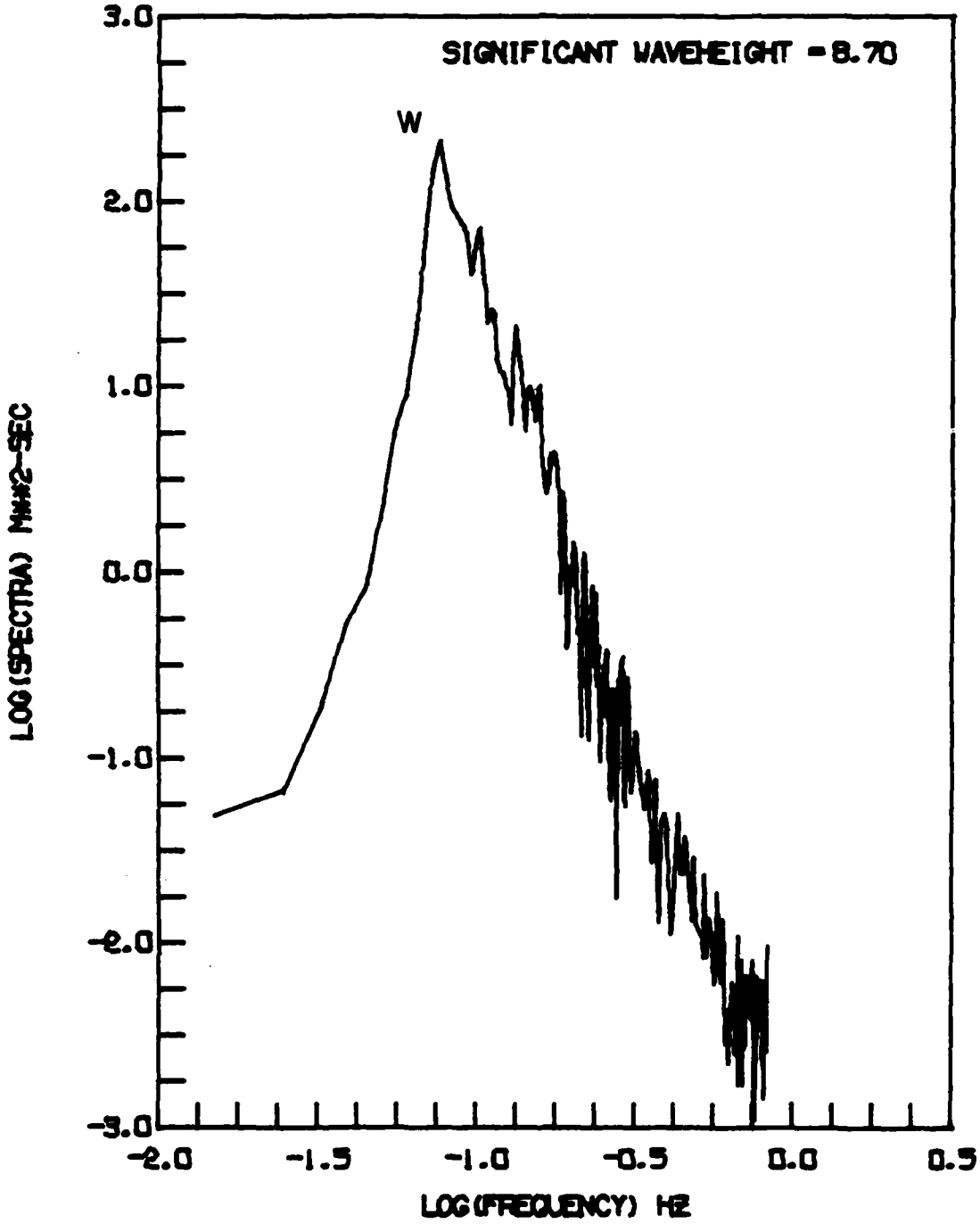

Fig. 7 - Ocean Wave Spectrum, Feb. 23b, 1976. For legend, see Fig. 4

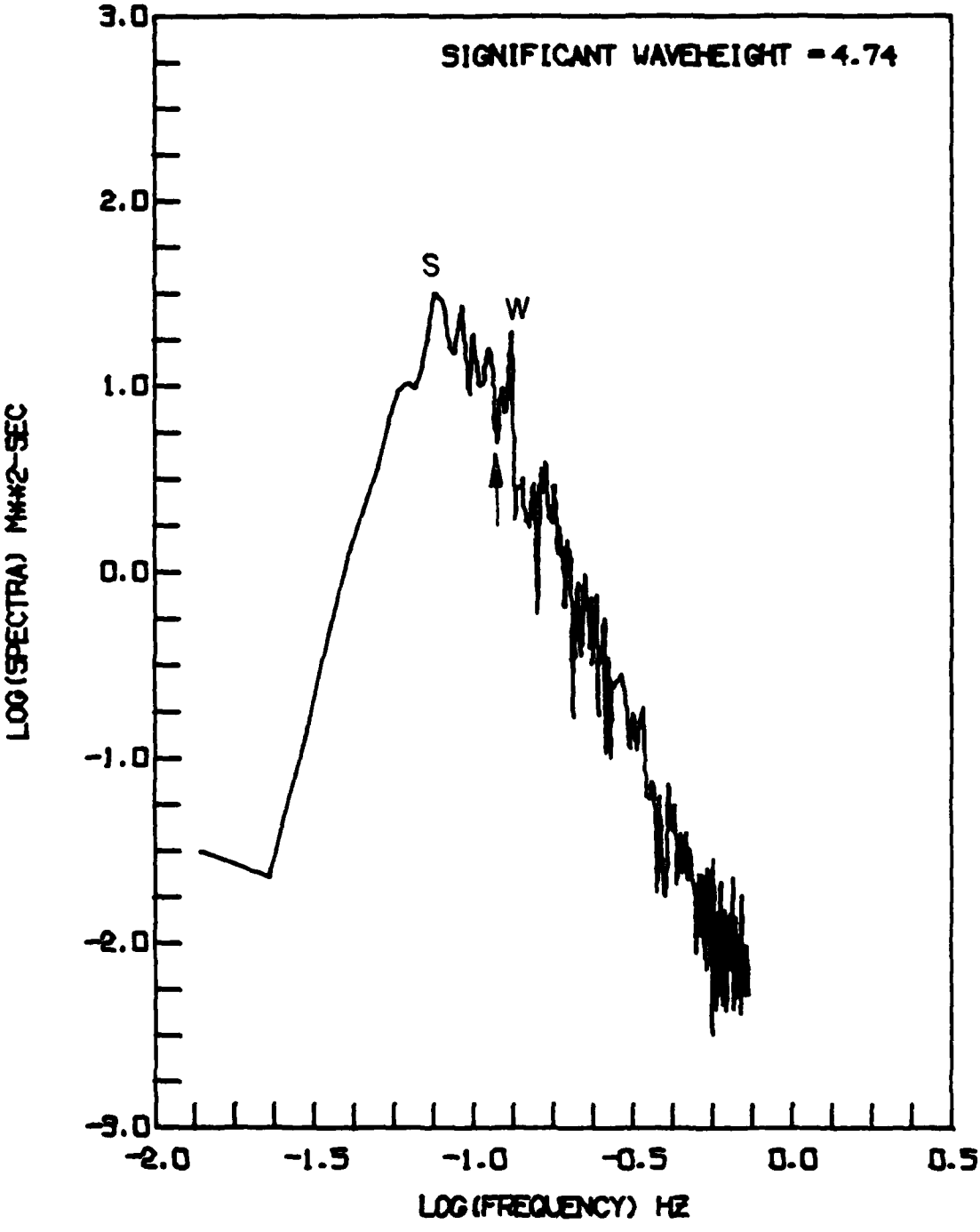

Fig. 8 - Ocean Wave Spectrum, Feb. 20, 1976. For legend, see Fig. 4

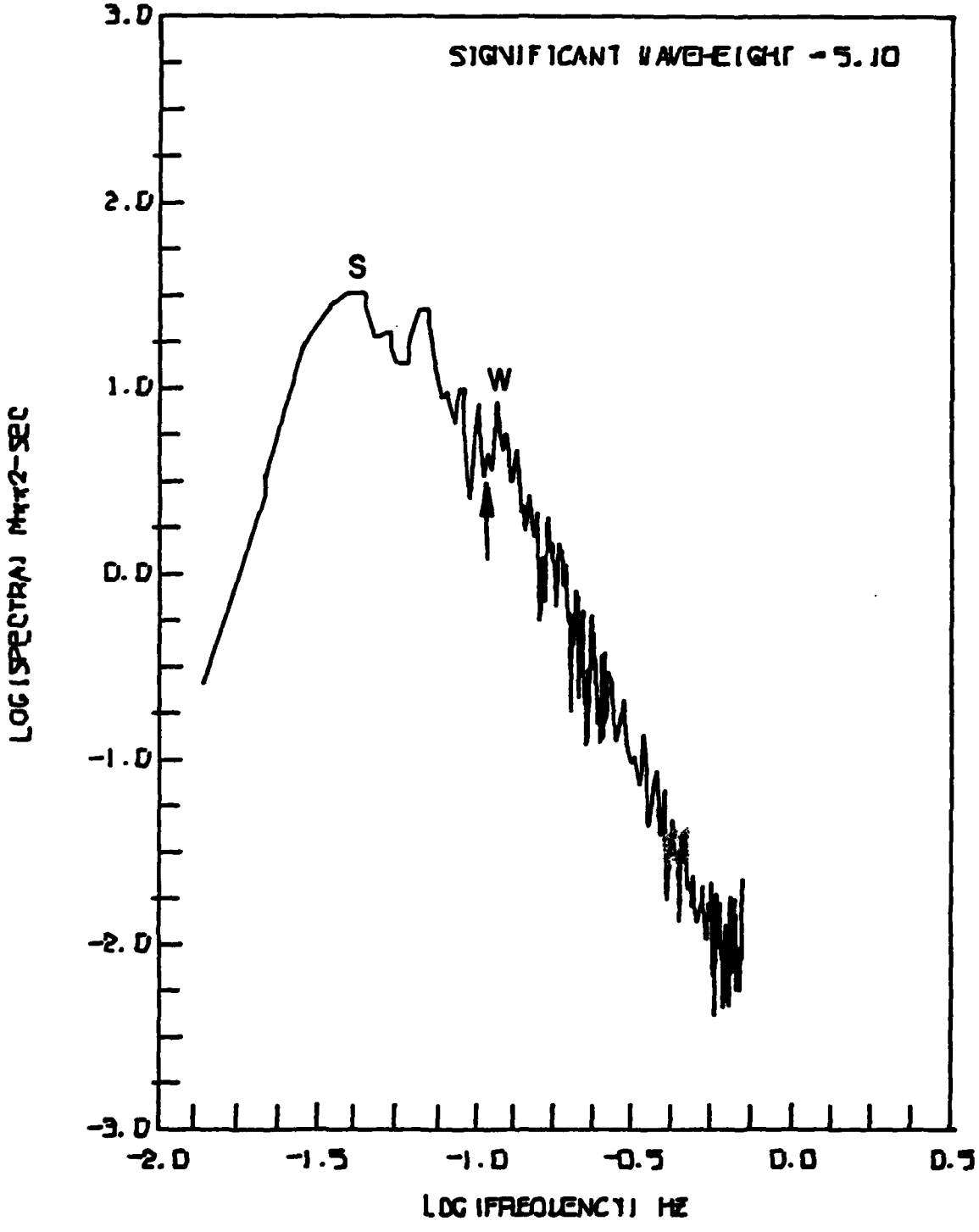

Fig. 9 - Ocean Wave Spectrum, Feb. 24, 1976. For legend, see Fig. 4

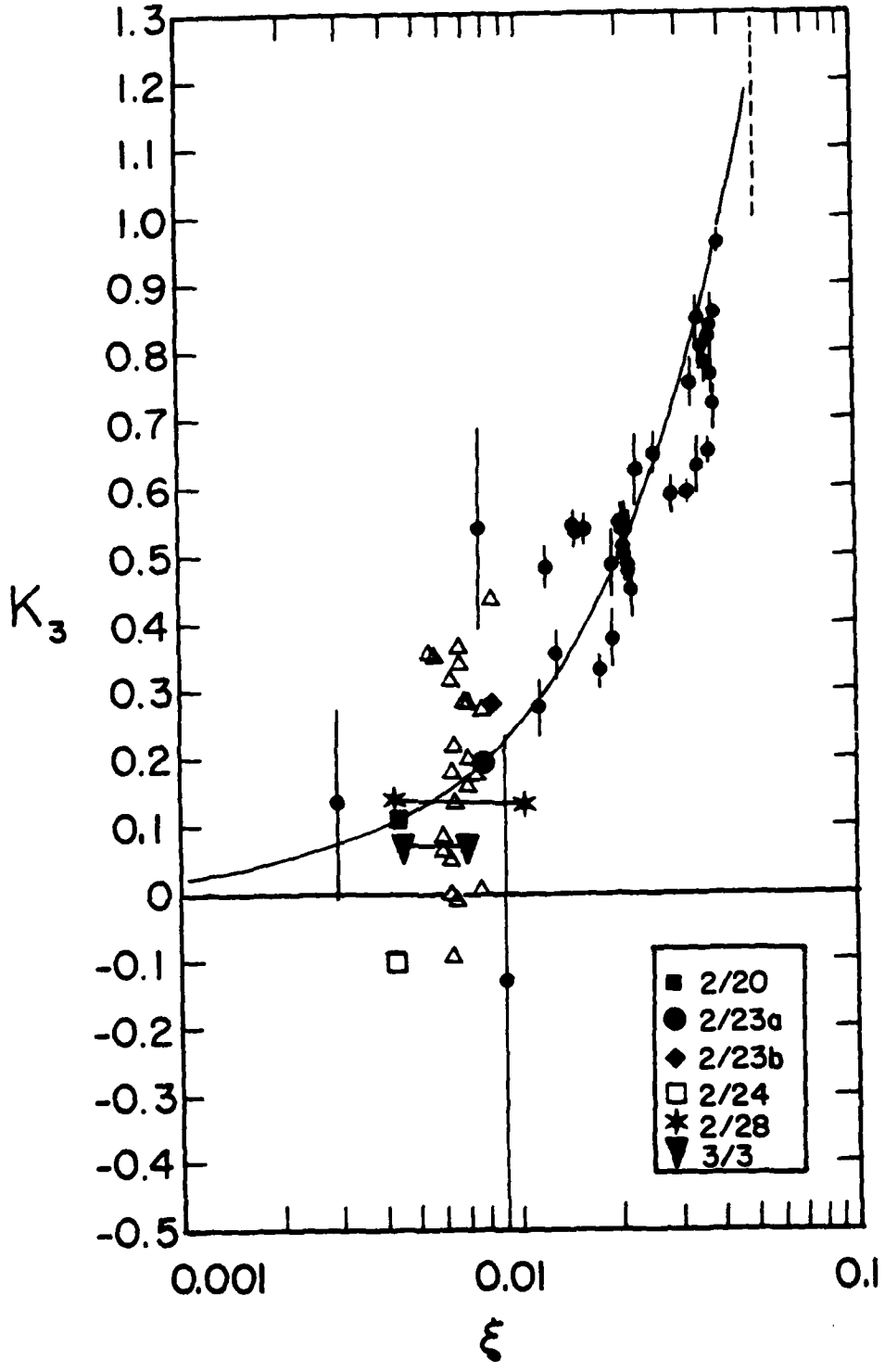

Fig. 10 - The Plot of Skewness K_3 with Significant Slope ξ. •, Data of the Wave Tank Study (Huang and Long, 1980), with One-Sigma Errors Bars; Δ, Results of In-Situ Field Study (Kinsman, 1960)

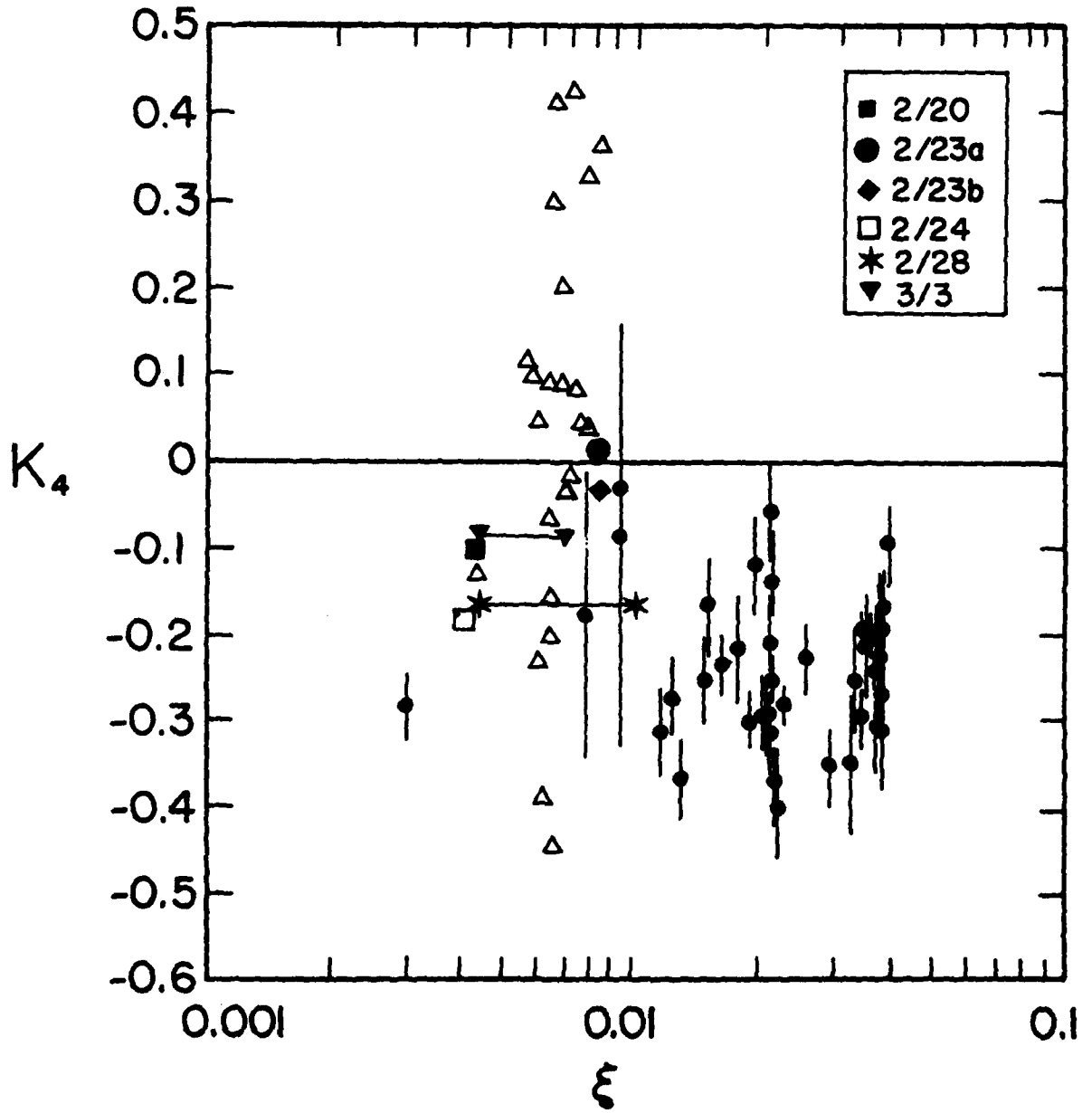

Fig. 11 - The Plot of Fourth-Order Cumulant K_4 with Significant Slope ξ. For legend, see Fig. 10

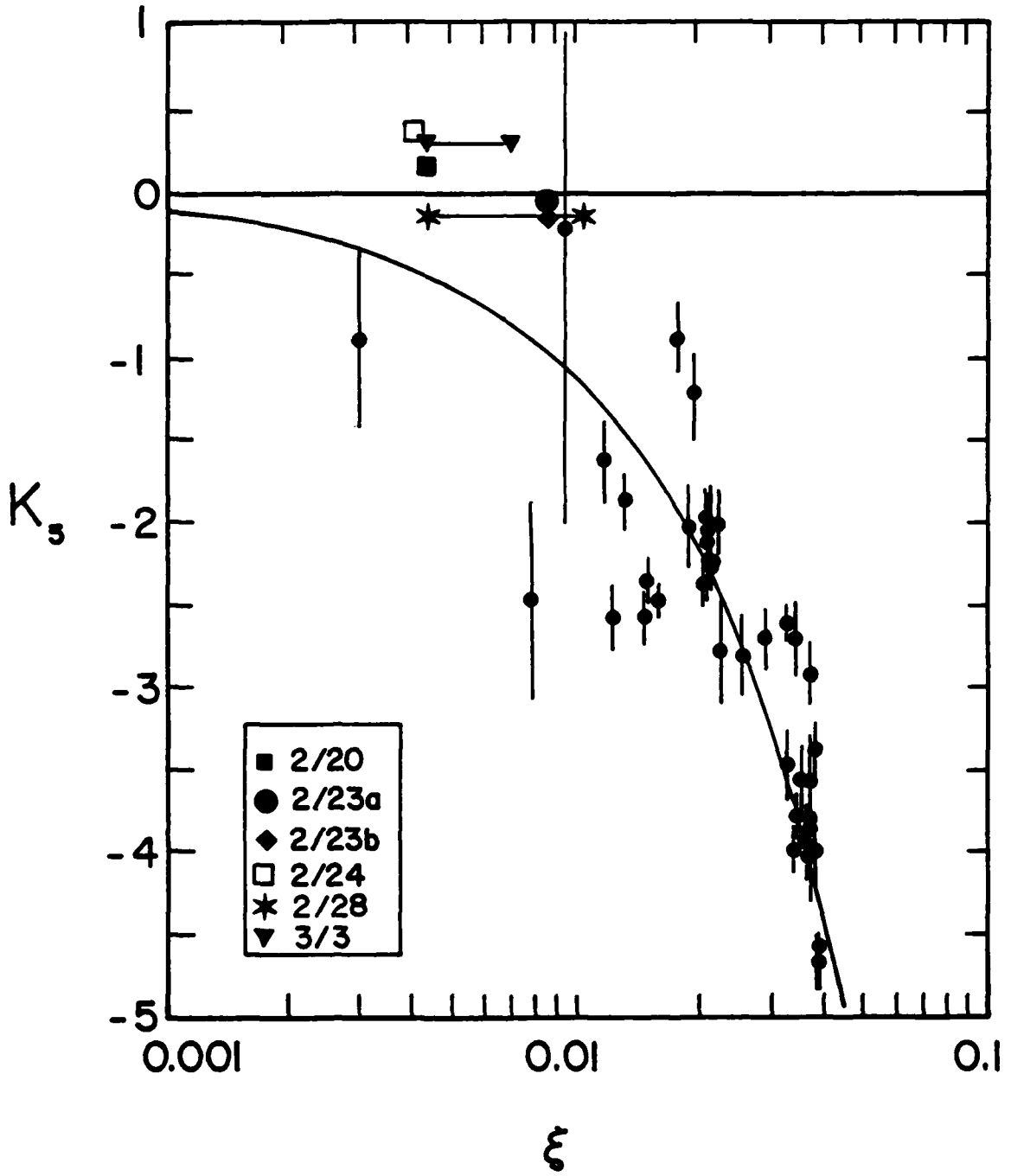

Fig. 12 - The Plot of Fifth-Order Cumulant K_5 with Significant Slope ξ. For legend, see Figure 10.

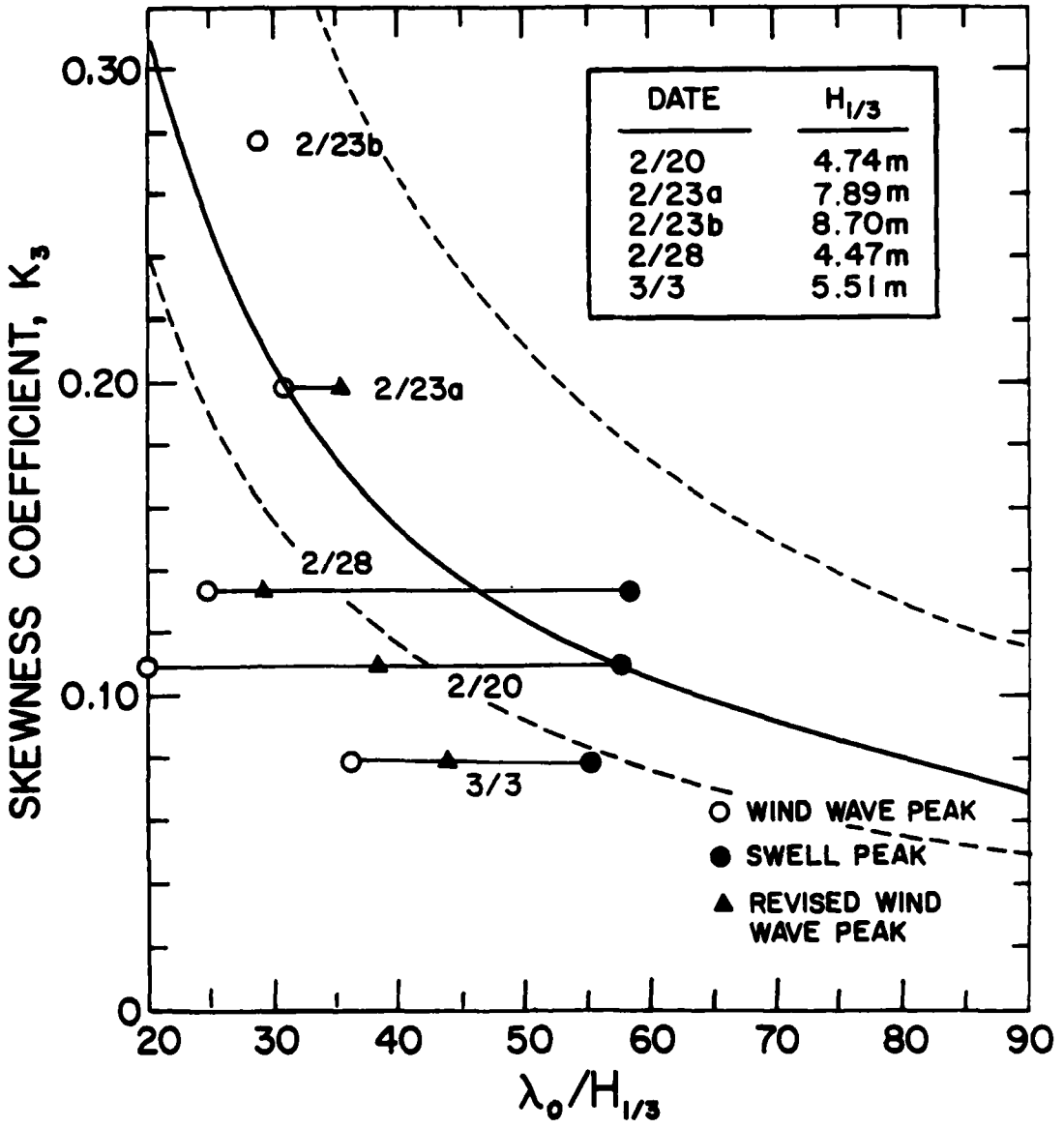

Fig. 13 - Empirical Relationship (Solid Curve), Theoretical Upper and Lower Bounds (Dotted Curves) between Skewness (Coefficient) K_3 and $\lambda_o/H_{1/3}$ with Swell, Wind-Wave, and Revised Wind-Wave Peaks for the Dates of 2/20, 2/23a, 2/23b, 2/28, and 3/3

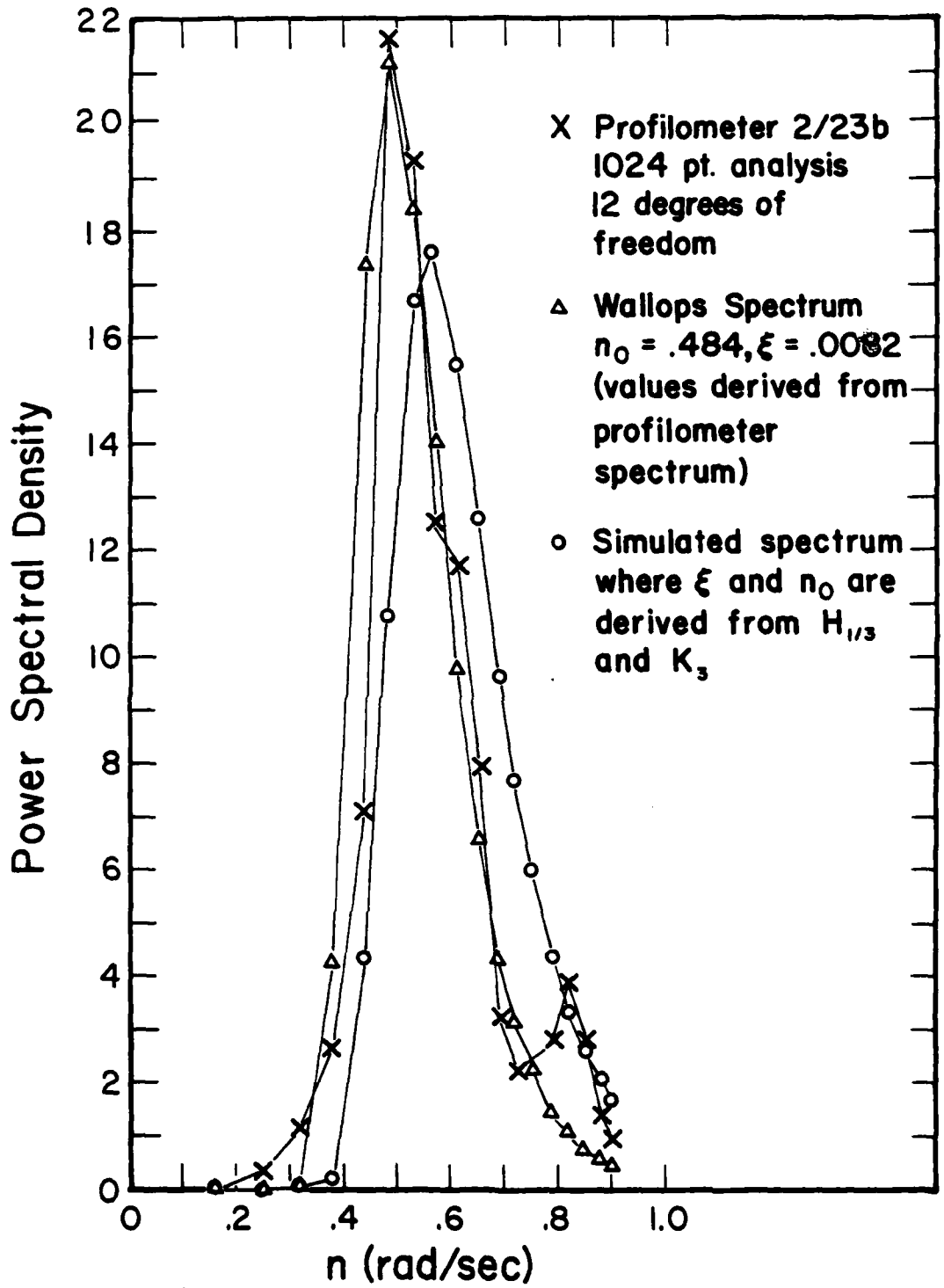

Fig. 14 - Ocean Wave Spectra Inferred by Wallops Spectral Model with Ocean Spectrum Measured on Feb. 23b, 1976

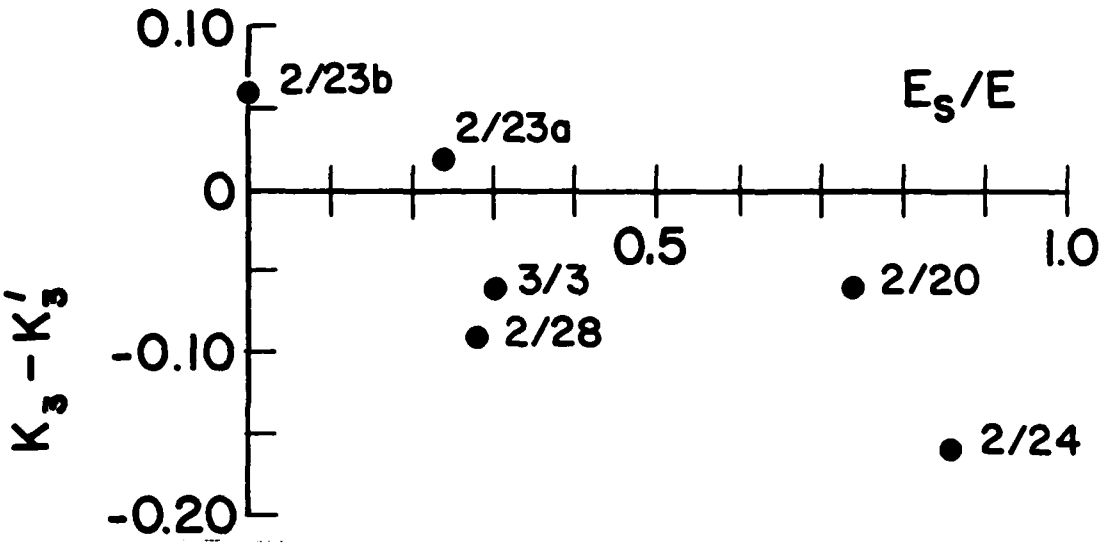

Fig. 15 - The Difference in Measured Skewness K_3 of the Combined Wave Field and the Predicted Skewness K'_3 for the Wind Wave Field as a Function of Relative Swell Energy

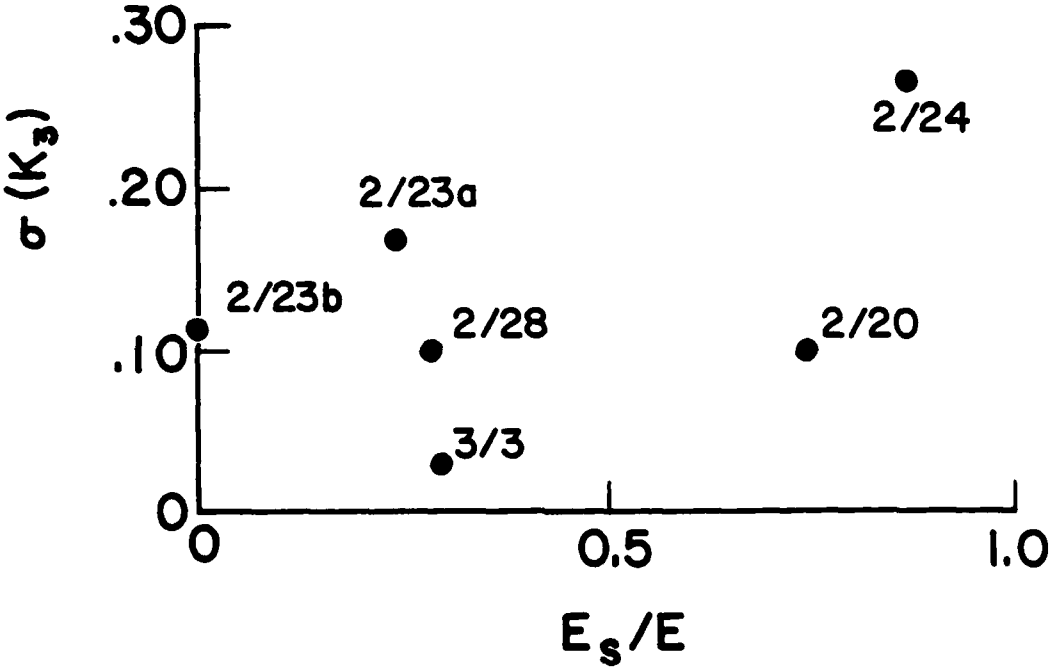

Fig. 16 - The Standard Deviation of Skewness Estimates as a Function of Relative Swell Energy, E_s/E

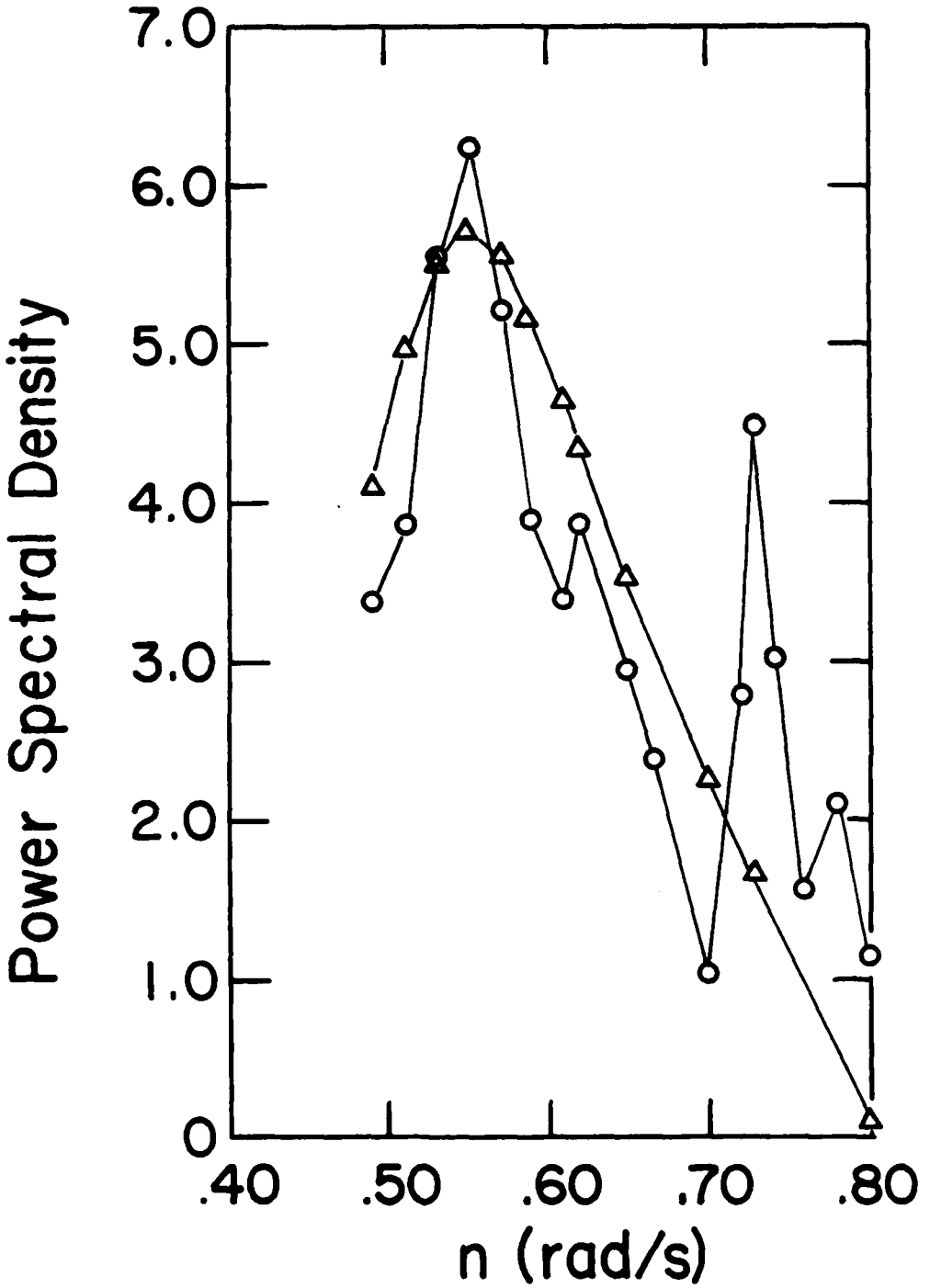

Fig. 17 - Comparison of Wallops Spectrum using Parameters Derived for the Wind Wave Field of March 3, 1976


DATE
ILME